EUROPEAN LABORATORY FOR PARTICLE PHYSICS (CERN)

CERN EP/98-017
5 February 1998

Resonant Structure and Flavour Tagging in the $B\pi^{\pm}$ System Using Fully Reconstructed B Decays

The ALEPH Collaboration*

Abstract

Starting from a sample of four million hadronic Z decays collected with the ALEPH detector at LEP, 404 charged and neutral B mesons are fully reconstructed and used to look for resonant structure in the $B\pi$ system. An excess of events is observed above the expected background in the $B\pi$ mass spectrum at a mass ≈ 5.7 GeV/c^2, consistent with the production and decay to $B^{(*)}\pi$ of the B^{**} states predicted by Heavy Quark Symmetry (HQS). In the framework of HQS, it is found that the mass of the B_2^* state is $(5739^{+\ 8}_{-11}(\mathrm{stat})^{+6}_{-4}(\mathrm{syst}))\,\mathrm{MeV/c^2}$ and the relative production rate of the B^{**} system is $BR(b \to B^{**} \to B^{(*)}\pi)/BR(b \to B_{u,d}) = (31 \pm 9(\mathrm{stat})^{+6}_{-5}(\mathrm{syst}))\%$. In the same sample of B mesons, significant $B\pi^{\pm}$ charge-flavour correlations are observed, which may prove important for tagging the initial B state in future CP violation studies.

(Submitted to Physics Letters B)

---

* See the following pages for the list of authors

The ALEPH Collaboration

R. Barate, D. Buskulic, D. Decamp, P. Ghez, C. Goy, J.-P. Lees, A. Lucotte, E. Merle, M.-N. Minard, J.-Y. Nief, B. Pietrzyk

Laboratoire de Physique des Particules (LAPP), IN^{2}P^3-CNRS, 74019 Annecy-le-Vieux Cedex, France

R. Alemany, G. Boix, M.P. Casado, M. Chmeissani, J.M. Crespo, M. Delfino, E. Fernandez, M. Fernandez-Bosman, Ll. Garrido,[15] E. Graugès, A. Juste, M. Martinez, G. Merino, R. Miquel, Ll.M. Mir, I.C. Park, A. Pascual, J.A. Perlas, I. Riu, F. Sanchez

Institut de Física d'Altes Energies, Universitat Autònoma de Barcelona, 08193 Bellaterra (Barcelona), Spain[7]

A. Colaleo, D. Creanza, M. de Palma, G. Gelao, G. Iaselli, G. Maggi, M. Maggi, S. Nuzzo, A. Ranieri, G. Raso, F. Ruggieri, G. Selvaggi, L. Silvestris, P. Tempesta, A. Tricomi,[3] G. Zito

Dipartimento di Fisica, INFN Sezione di Bari, 70126 Bari, Italy

X. Huang, J. Lin, Q. Ouyang, T. Wang, Y. Xie, R. Xu, S. Xue, J. Zhang, L. Zhang, W. Zhao

Institute of High-Energy Physics, Academia Sinica, Beijing, The People's Republic of China[8]

D. Abbaneo, U. Becker, P. Bright-Thomas, D. Casper, M. Cattaneo, V. Ciulli, G. Dissertori, H. Drevermann, R.W. Forty, M. Frank, R. Hagelberg, J.B. Hansen, J. Harvey, R. Jacobsen,[26] P. Janot, B. Jost, I. Lehraus, P. Mato, A. Minten, L. Moneta,[21] A. Pacheco, J.-F. Pusztaszeri,[23] F. Ranjard, L. Rolandi, D. Rousseau, D. Schlatter, M. Schmitt,[25] O. Schneider, W. Tejessy, F. Teubert, I.R. Tomalin, H. Wachsmuth, A. Wagner[20]

European Laboratory for Particle Physics (CERN), 1211 Geneva 23, Switzerland

Z. Ajaltouni, F. Badaud, G. Chazelle, O. Deschamps, A. Falvard, C. Ferdi, P. Gay, C. Guicheney, P. Henrard, J. Jousset, B. Michel, S. Monteil, J-C. Montret, D. Pallin, P. Perret, F. Podlyski, J. Proriol, P. Rosnet

Laboratoire de Physique Corpusculaire, Université Blaise Pascal, IN^{2}P^3-CNRS, Clermont-Ferrand, 63177 Aubière, France

J.D. Hansen, J.R. Hansen, P.H. Hansen, B.S. Nilsson, B. Rensch, A. Wäänänen

Niels Bohr Institute, 2100 Copenhagen, Denmark[9]

G. Daskalakis, A. Kyriakis, C. Markou, E. Simopoulou, I. Siotis, A. Vayaki

Nuclear Research Center Demokritos (NRCD), Athens, Greece

A. Blondel, G. Bonneaud, J.-C. Brient, P. Bourdon, A. Rougé, M. Rumpf, A. Valassi,[6] M. Verderi, H. Videau

Laboratoire de Physique Nucléaire et des Hautes Energies, Ecole Polytechnique, IN^{2}P^3-CNRS, 91128 Palaiseau Cedex, France

E. Focardi, G. Parrini, K. Zachariadou

Dipartimento di Fisica, Università di Firenze, INFN Sezione di Firenze, 50125 Firenze, Italy

M. Corden, C. Georgiopoulos, D.E. Jaffe

Supercomputer Computations Research Institute, Florida State University, Tallahassee, FL 32306-4052, USA [13,14]

A. Antonelli, G. Bencivenni, G. Bologna,[4] F. Bossi, P. Campana, G. Capon, F. Cerutti, V. Chiarella, G. Felici, P. Laurelli, G. Mannocchi,[5] F. Murtas, G.P. Murtas, L. Passalacqua, M. Pepe-Altarelli

Laboratori Nazionali dell'INFN (LNF-INFN), 00044 Frascati, Italy

L. Curtis, A.W. Halley, J.G. Lynch, P. Negus, V. O'Shea, C. Raine, J.M. Scarr, K. Smith, P. Teixeira-Dias, A.S. Thompson, E. Thomson

Department of Physics and Astronomy, University of Glasgow, Glasgow G12 8QQ,United Kingdom[10]

O. Buchmüller, S. Dhamotharan, C. Geweniger, G. Graefe, P. Hanke, G. Hansper, V. Hepp, E.E. Kluge, A. Putzer, J. Sommer, K. Tittel, S. Werner, M. Wunsch

Institut für Hochenergiephysik, Universität Heidelberg, 69120 Heidelberg, Fed. Rep. of Germany[16]

R. Beuselinck, D.M. Binnie, W. Cameron, P.J. Dornan,[2] M. Girone, S. Goodsir, E.B. Martin, N. Marinelli, A. Moutoussi, J. Nash, J.K. Sedgbeer, P. Spagnolo, M.D. Williams

Department of Physics, Imperial College, London SW7 2BZ, United Kingdom[10]

V.M. Ghete, P. Girtler, E. Kneringer, D. Kuhn, G. Rudolph

Institut für Experimentalphysik, Universität Innsbruck, 6020 Innsbruck, Austria[18]

A.P. Betteridge, C.K. Bowdery, P.G. Buck, P. Colrain, G. Crawford, A.J. Finch, F. Foster, G. Hughes, R.W.L. Jones, M.I. Williams

Department of Physics, University of Lancaster, Lancaster LA1 4YB, United Kingdom[10]

I. Giehl, A.M. Greene, C. Hoffmann, K. Jakobs, K. Kleinknecht, G. Quast, B. Renk, E. Rohne, H.-G. Sander, P. van Gemmeren, C. Zeitnitz

Institut für Physik, Universität Mainz, 55099 Mainz, Fed. Rep. of Germany[16]

J.J. Aubert, C. Benchouk, A. Bonissent, G. Bujosa, D. Calvet, J. Carr,[2] P. Coyle, F. Etienne, O. Leroy, F. Motsch, P. Payre, M. Talby, A. Sadouki, M. Thulasidas, K. Trabelsi

Centre de Physique des Particules, Faculté des Sciences de Luminy, IN^{2}P^3-CNRS, 13288 Marseille, France

M. Aleppo, M. Antonelli, F. Ragusa

Dipartimento di Fisica, Università di Milano e INFN Sezione di Milano, 20133 Milano, Italy

R. Berlich, W. Blum, V. Büscher, H. Dietl, G. Ganis, H. Kroha, G. Lütjens, C. Mannert, W. Männer, H.-G. Moser, S. Schael, R. Settles, H. Seywerd, H. Stenzel, W. Wiedenmann, G. Wolf

Max-Planck-Institut für Physik, Werner-Heisenberg-Institut, 80805 München, Fed. Rep. of Germany[16]

J. Boucrot, O. Callot, S. Chen, A. Cordier, M. Davier, L. Duflot, J.-F. Grivaz, Ph. Heusse, A. Höcker, A. Jacholkowska, D.W. Kim,[12] F. Le Diberder, J. Lefrançois, A.-M. Lutz, M.-H. Schune, E. Tournefier, J.-J. Veillet, I. Videau, D. Zerwas

Laboratoire de l'Accélérateur Linéaire, Université de Paris-Sud, IN^{2}P^3-CNRS, 91405 Orsay Cedex, France

P. Azzurri, G. Bagliesi,[2] G. Batignani, S. Bettarini, T. Boccali, C. Bozzi, G. Calderini, M. Carpinelli, M.A. Ciocci, R. Dell'Orso, R. Fantechi, I. Ferrante, L. Foà,[1] F. Forti, A. Giassi, M.A. Giorgi, A. Gregorio, F. Ligabue, A. Lusiani, P.S. Marrocchesi, A. Messineo, F. Palla, G. Rizzo, G. Sanguinetti, A. Sciabà, R. Tenchini, G. Tonelli,[19] C. Vannini, A. Venturi, P.G. Verdini

Dipartimento di Fisica dell'Università, INFN Sezione di Pisa, e Scuola Normale Superiore, 56010 Pisa, Italy

G.A. Blair, L.M. Bryant, J.T. Chambers, M.G. Green, T. Medcalf, P. Perrodo, J.A. Strong, J.H. von Wimmersperg-Toeller

Department of Physics, Royal Holloway & Bedford New College, University of London, Surrey TW20 OEX, United Kingdom[10]

D.R. Botterill, R.W. Clifft, T.R. Edgecock, S. Haywood, P.R. Norton, J.C. Thompson, A.E. Wright

Particle Physics Dept., Rutherford Appleton Laboratory, Chilton, Didcot, Oxon OX11 OQX, United Kingdom[10]

B. Bloch-Devaux, P. Colas, S. Emery, W. Kozanecki, E. Lançon,[2] M.-C. Lemaire, E. Locci, P. Perez, J. Rander, J.-F. Renardy, A. Roussarie, J.-P. Schuller, J. Schwindling, A. Trabelsi, B. Vallage

CEA, DAPNIA/Service de Physique des Particules, CE-Saclay, 91191 Gif-sur-Yvette Cedex, France[17]

S.N. Black, J.H. Dann, R.P. Johnson, H.Y. Kim, N. Konstantinidis, A.M. Litke, M.A. McNeil, G. Taylor

Institute for Particle Physics, University of California at Santa Cruz, Santa Cruz, CA 95064, USA[22]

C.N. Booth, C.A.J. Brew, S. Cartwright, F. Combley, M.S. Kelly, M. Lehto, J. Reeve, L.F. Thompson

Department of Physics, University of Sheffield, Sheffield S3 7RH, United Kingdom[10]

K. Affholderbach, A. Böhrer, S. Brandt, G. Cowan, C. Grupen, P. Saraiva, L. Smolik, F. Stephan

Fachbereich Physik, Universität Siegen, 57068 Siegen, Fed. Rep. of Germany[16]

M. Apollonio, L. Bosisio, R. Della Marina, G. Giannini, B. Gobbo, G. Musolino

Dipartimento di Fisica, Università di Trieste e INFN Sezione di Trieste, 34127 Trieste, Italy

J. Rothberg, S. Wasserbaech

Experimental Elementary Particle Physics, University of Washington, WA 98195 Seattle, U.S.A.

S.R. Armstrong, E. Charles, P. Elmer, D.P.S. Ferguson, Y. Gao, S. González, T.C. Greening, O.J. Hayes, H. Hu, S. Jin, P.A. McNamara III, J.M. Nachtman,[24] J. Nielsen, W. Orejudos, Y.B. Pan, Y. Saadi, I.J. Scott, J. Walsh, Sau Lan Wu, X. Wu, G. Zobernig

Department of Physics, University of Wisconsin, Madison, WI 53706, USA[11]

---

[1]Now at CERN, 1211 Geneva 23, Switzerland.
[2]Also at CERN, 1211 Geneva 23, Switzerland.
[3]Also at Dipartimento di Fisica, INFN, Sezione di Catania, Catania, Italy.
[4]Also Istituto di Fisica Generale, Università di Torino, Torino, Italy.
[5]Also Istituto di Cosmo-Geofisica del C.N.R., Torino, Italy.
[6]Supported by the Commission of the European Communities, contract ERBCHBICT941234.
[7]Supported by CICYT, Spain.
[8]Supported by the National Science Foundation of China.
[9]Supported by the Danish Natural Science Research Council.
[10]Supported by the UK Particle Physics and Astronomy Research Council.
[11]Supported by the US Department of Energy, grant DE-FG0295-ER40896.
[12]Permanent address: Kangnung National University, Kangnung, Korea.
[13]Supported by the US Department of Energy, contract DE-FG05-92ER40742.
[14]Supported by the US Department of Energy, contract DE-FC05-85ER250000.
[15]Permanent address: Universitat de Barcelona, 08208 Barcelona, Spain.
[16]Supported by the Bundesministerium für Bildung, Wissenschaft, Forschung und Technologie, Fed. Rep. of Germany.
[17]Supported by the Direction des Sciences de la Matière, C.E.A.
[18]Supported by Fonds zur Förderung der wissenschaftlichen Forschung, Austria.
[19]Also at Istituto di Matematica e Fisica, Università di Sassari, Sassari, Italy.
[20]Now at Schweizerischer Bankverein, Basel, Switzerland.
[21]Now at University of Geneva, 1211 Geneva 4, Switzerland.
[22]Supported by the US Department of Energy, grant DE-FG03-92ER40689.
[23]Now at School of Operations Research and Industrial Engineering, Cornell University, Ithaca, NY 14853-3801, U.S.A.
[24]Now at University of California at Los Angeles (UCLA), Los Angeles, CA 90024, U.S.A.
[25]Now at Harvard University, Cambridge, MA 02138, U.S.A.
[26]Now at Lawrence Berkeley Laboratory, California, CA 94720, U.S.A.

1 Introduction

The ability to tag the flavour of neutral B mesons at production by the charge of a near-by pion [1] has important implications for the study of CP violation and mixing in the B^0 system. This flavour tagging ability is enhanced by the existence of resonant structure in the $B^{(*)}\pi$ system. The first such resonances expected to be observed are the $\ell = 1$ orbitally excited B states, generically called B^{**}. The masses, widths, and decay branching ratios of these states have been the subject of theoretical predictions, based on Heavy Quark Symmetry (HQS) and extrapolation from the measured properties of the analogous D^{**} states [2].

For $\ell = 1$, four states are expected. According to HQS, these are grouped into two doublets which are characterised by the total angular momentum of the light quark $\vec{j}_q = \vec{\ell} + \vec{s}_q$. The $j_q = 1/2$ doublet consists of the states B_0 and B_1^*, with spins 0 and 1 respectively. The states B_1 and B_2^*, with respective spins 1 and 2, comprise the $j_q = 3/2$ doublet. The mass splitting between the states in each doublet is expected to be small ($\sim 10\,\mathrm{MeV/c^2}$), while the two doublets are expected to have a mass difference of the order of $100\,\mathrm{MeV/c^2}$. Due to parity and angular momentum conservation, the states with $j_q = 3/2$ can decay to $B^{(*)}\pi$ only via a D-wave and therefore are expected to be narrow ($\Gamma \sim 20\,\mathrm{MeV/c^2}$), whereas the decays to $B^{(*)}\pi$ of the $j_q = 1/2$ states can proceed via S-waves giving rise to large decay widths ($\Gamma \sim 150\,\mathrm{MeV/c^2}$).

The first experimental results on excited B states came from experiments at LEP, where the B mesons are produced in the decays $Z \to b\bar{b}$. Evidence for $B\pi$ charge correlations [3] and $B\pi$ resonant structure [3, 4, 5] have been observed. However, all these studies are based on the inclusive reconstruction of B mesons. The resulting $B\pi$ mass resolution is poor (of the order of $40\,\mathrm{MeV}/c^2$), and the assignment of tracks to the B is not unambiguous.

In this paper a different, complementary approach is presented. Charged and neutral B mesons, fully reconstructed in the ALEPH experiment at LEP, are used to study $B\pi$ resonant structure and charge-flavour correlations. The advantage of this approach for the study of the B^{**} states is that the mass resolution is improved by about one order of magnitude compared to the previous studies, allowing the observation of narrower structure. The advantage for the study of flavour tagging and mixing is that this method corresponds much more closely to the techniques that have been proposed for future experiments on CP violation, which depend on the full reconstruction of neutral B mesons. Moreover, the identity and decay proper time of the B meson are accurately known, and there is a clean separation between tracks from the B decay and tracks from fragmentation.

The disadvantage of this approach with the present data sample is the limited number of fully reconstructed B mesons. The results presented here are based on about four million hadronic Z decays, collected by the ALEPH detector from 1991 to 1995. This data sample yields 404 fully reconstructed B meson candidates in a variety of hadronic decay modes.

The outline of this paper is as follows: after a brief description of the detector in section 2 and the reconstruction of B candidates in section 3, the $B\pi$ mass spectrum is studied in section 4; an excess of events, observed at a mass of $\approx 5.7\,\mathrm{GeV/c^2}$, is first fitted with a single Gaussian and later with a spectrum of B^{**} states in the context of HQS. The B flavour tagging is detailed

in section 5 and section 6 gives the conclusions.

2 The ALEPH Detector

The ALEPH detector and its performance are described in detail elsewhere [6, 7]. Only a brief description of the parts of the apparatus most important for this analysis is given in this section. The most critical elements are the charged particle tracking, especially the silicon vertex detector, and the particle identification with dE/dx.

Charged particles are tracked with three concentric devices which reside inside a superconducting solenoidal magnet. The vertex detector (VDET) [8] consists of double-sided silicon microstrip detectors with strip readout in two orthogonal directions. The strip detectors are arranged in two cylindrical layers at average radii of 6.3 and 10.8 cm, with solid angle coverage of $|\cos\theta| < 0.85$ for the inner layer and $|\cos\theta| < 0.69$ for both layers. The spatial resolution is 12 μm in the $r\phi$ coordinate, and varies from 12 μm to 22 μm in the rz coordinate depending on the track polar angle. Surrounding the VDET is the inner tracking chamber (ITC), a cylindrical drift chamber with up to eight measurements in the $r\phi$ dimension from radii of 16 to 26 cm. Outside the ITC, the time projection chamber (TPC) provides up to 21 three-dimensional coordinates per track for radii between 40 and 171 cm.

With the axial magnetic field of 1.5 T the transverse momentum resolution of the tracking system is given by $\sigma(p_T)/p_T = 6 \times 10^{-4} p_T \oplus 0.005$ (p_T in GeV/c). The impact parameter resolution, for tracks with VDET hits in both layers, can be parametrized as a function of momentum as $\sigma(\delta) = (25 + 95/p)$ μm in both the $r\phi$ and rz views, with p in GeV/c.

In addition to tracking, the TPC is used for particle identification by measurement of the specific ionization energy loss dE/dx associated with each charged track; it provides up to 338 dE/dx measurements. For particles produced in hadronic Z decays, in the relativistic rise region with at least 50 dE/dx measurements, the separation between pions and kaons is approximately two standard deviations.

3 B Candidate Reconstruction

Charged and neutral B mesons are fully reconstructed in a variety of hadronic decay channels. Eighty percent are in the mode[1] $B \to D^{(*)}X$, where X is a charged π, ρ or a_1, and 20% are of the form $B \to J/\psi(\psi')X$, where X is a charged K or a neutral K^*. The reconstruction follows the analysis described in reference [9] with the addition of lifetime related cuts, and the modification of other cuts intended to increase the event yield. The resulting B mass spectrum is shown in Fig. 1.

In addition, charged B candidates are reconstructed in the channels $B^- \to D^{*0}\pi^-$ and

[1] Throughout this paper, charge conjugate decay modes are always implied.

$D^{*0}a_1^-$, with a missing soft γ or π^0 from the $D^{*0} \to D^0\gamma$ or $D^0\pi^0$ decays. These candidates form the broad structure, visible in Fig. 1, about 200 MeV/c^2 below the nominal B mass. The loss of the soft neutral particle is accounted for by scaling the mass and momentum of the D^0 candidate to the mass and average momentum of the D^{*0}. These candidates give a $B\pi$ mass resolution comparable to that achieved with the fully reconstructed B candidates.

In total, 238 charged and 166 neutral B candidates are collected. The purities, $(84 \pm 3\,\%)$ and $(86 \pm 3\,\%)$ respectively, are measured by fitting exponential backgrounds and Gaussian signals to the mass spectra, as seen in Fig. 1. These candidates have very good momentum and proper time resolution ($\Delta p/p \approx 1\%$, $\Delta t \approx 0.1$ ps [9]), which are relevant for the study of $B\pi$ spectroscopy and B flavour tagging.

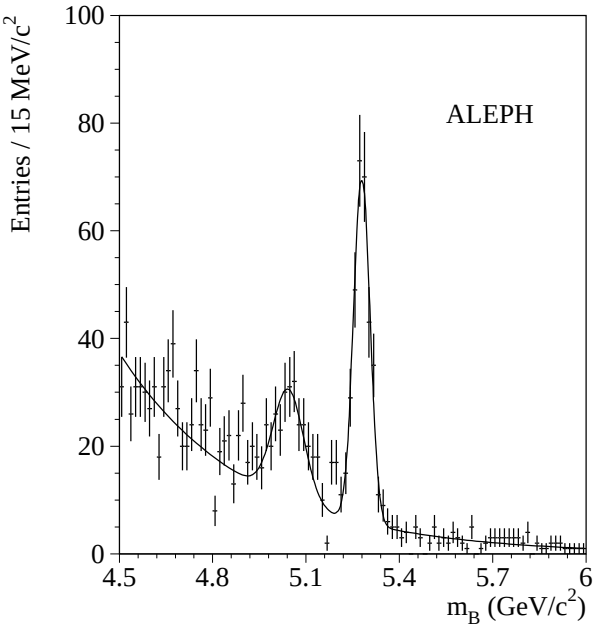

Figure 1: The B mass spectrum including all decay channels. Also shown is the fit to the signal plus background.

4 B^{**} Spectroscopy

4.1 $B^{**} \to B^{(*)}\pi^{\pm}$ Candidate Selection

B^{**} resonant states are searched for in the decay mode $B^{**} \to B^{(*)}\pi^{\pm}$. Charged tracks which are not used in the reconstruction of the B meson are potential candidates for the associated charged π (which will be referred to as the π_{**}). The π_{**} candidate track must have a momentum > 0.2 GeV/c, originate from the primary vertex (with a probability $\geq 0.5\%$), and have an ionization energy loss consistent with a pion within 3 standard deviations (provided there are ≥ 50 dE/dx measurements).

Tracks passing the above selection are then classified as *'right-sign'* or *'wrong-sign'*, according to their charge. For a specific B hadron type, only right-sign tracks can originate from the decay of a B^{**} resonance into $B\pi$. Positive tracks are right-sign for B^- and B^0 candidates, while negative tracks are right-sign for B^+'s and $\bar{B}^0$'s. The distinction between right-sign and wrong-sign tracks reduces the background combinations by almost a factor of two, with only a small reduction in the signal efficiency due to $B^0 - \bar{B}^0$ mixing. Furthermore, the wrong-sign combinations serve as a check on the estimate of the background and the reliability of the simulation.

The majority of the remaining tracks come from fragmentation. The signal pions are expected to be more 'forward' and energetic than fragmentation tracks. Therefore, the π_{**} candidate in each event is chosen to be the right-sign track with the highest component of momentum along the direction of the B and, in addition, gives an invariant mass in combination with the B of less than $7.3\,\mathrm{GeV/c^2}$ (the P_L^{max} track). The requirement of $M(B\pi) < 7.3\,\mathrm{GeV/c^2}$ increases the probability to select the signal π_{**} as opposed to hard tracks from nearby gluon jets in events with more than two jets. The overall efficiency for the signal (after applying the P_L^{max} algorithm) is estimated from simulation to be $(63 \pm 4)\%$. Choosing the wrong-sign P_L^{max} track instead provides a useful control sample. Constraining the B mass to its nominal value [10], the $B\pi$ invariant mass resolution varies from 2 to $5\,\mathrm{MeV/c^2}$ in the $B\pi$ mass range from 5.5 to $5.8\,\mathrm{GeV/c^2}$.

4.2 $B\pi^{\pm}$ Mass Distribution

The $B\pi$ mass distributions for right-sign and wrong-sign combinations in the data, based on the P_L^{max} algorithm, are shown in Fig. 2. The expected mass distribution of the background is also indicated. The shape of the background from true B's combined with fragmentation tracks is estimated using simulated events. The shape of the background coming from *fake* B candidates (which make up the $(15 \pm 3)\%$ impurity of the B sample) is determined from the data, using a sample of *fake* B candidates collected from the high mass sideband of the B mass spectrum. These two shapes are added together, weighted by their estimated relative contributions, to give the overall background shape. The normalization of the background in the right-sign distribution is based on the number of events in the high mass region, above $6\,\mathrm{GeV/c^2}$, where no significant contribution from B^{**} resonances is expected. The normalization for the wrong-sign distribution is based on the total number of events in the histogram.

It can be seen in Fig. 2b that there is good agreement in shape for the wrong-sign distribution, where only a small fraction of B^{**} is expected due to mixing. In the right-sign distribution, however, there is a significant excess of events around $5.7\,\mathrm{GeV/c^2}$ above the expected background.

A structure in the $B\pi$ invariant mass in the region between 5.6 and $5.8\,\mathrm{GeV/c^2}$ has previously been observed in inclusive B plus pion studies at LEP [3, 4, 5]. This mass range is chosen to estimate the statistical significance of the excess: 106 events are observed, while 65 ± 6 events are expected from background (with the error calculated from the statistical error on the

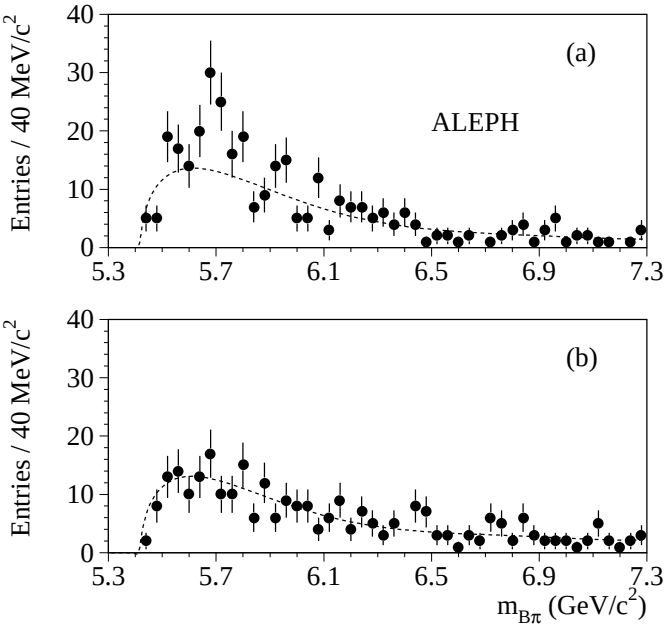

Figure 2: The $B\pi$ mass distributions in the data with the expected background shapes: (a) right-sign mass distribution and (b) wrong-sign mass distribution.

normalization). The probability for the expected background to fluctuate up to at least the observed number of events is 2×10^{-5}.

An unbinned likelihood fit is used to extract the characteristics of the observed excess at $\approx 5.7\,\mathrm{GeV/c^2}$ in the right-sign distribution. Below $6\,\mathrm{GeV/c^2}$, the fitting function includes a Poisson probability factor for the observed number of events, the background shape (as described above), plus a single Gaussian (to permit comparison with earlier results [3, 4, 5]). Above $6\,\mathrm{GeV/c^2}$, a normalizing Poisson probability factor for the total number of events between 6.0 and $7.3\,\mathrm{GeV/c^2}$ is employed. The results of the fit, shown in Fig. 3, are: mass $= (5695^{+17}_{-19})\,\mathrm{MeV/c^2}$, width $\sigma = (53^{+26}_{-19})\,\mathrm{MeV/c^2}$ and total area of the Gaussian $= 43^{+17}_{-14}$ events. Systematic errors are estimated to be small relative to the quoted statistical errors.

Attributing the observed signal, as represented by the total area of the Gaussian, to the production of $B^{(*)}\pi$ resonant states, and including the efficiency of the P_L^{max} algorithm and the purity of the B sample, the relative production rate for these states is calculated to be:

$$\frac{BR(b \to B^{(*)}\pi \text{ resonant})}{BR(b \to B_{u,d})} = (30^{+12}_{-10}(\mathrm{stat}) \pm 3(\mathrm{syst}))\%.$$

The calculation also includes an isospin factor of 2/3 to take account of the unobserved $B^{(*)}\pi^0$ decays. The systematic error is dominated by the uncertainties on the efficiency of the P_L^{max} algorithm and on the purity of the B sample. It also includes uncertainties in the background shape which were studied by varying relevant fragmentation parameters in the simulation. These results on mass, width and production rate are in agreement with the previous observations [3, 4, 5].

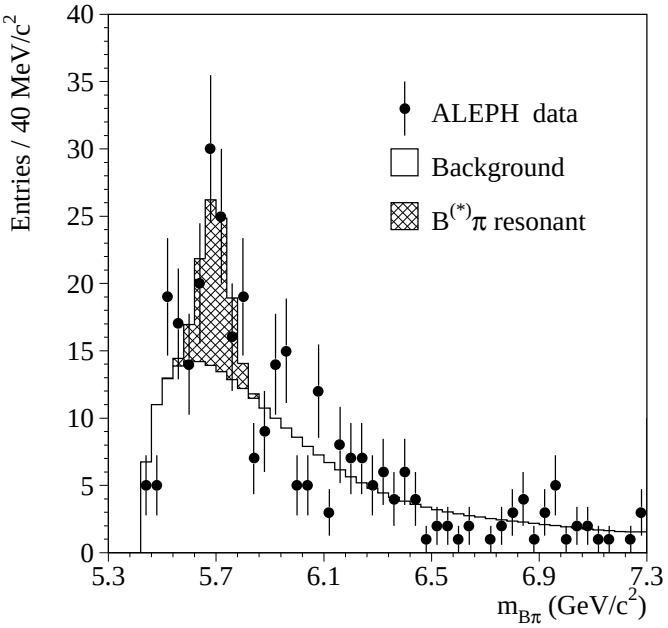

Figure 3: The right-sign $B\pi$ mass distribution from data with the results of a fit based on the expected background and a single Gaussian distribution.

4.3 $B\pi$ Mass Distribution and HQS Predictions

In the framework of HQS, the contribution of the B^{**} states to the $B\pi$ mass spectrum is expected to be considerably more complex than a single Gaussian as was assumed in section 4.2. As mentioned in the introduction, four $\ell = 1$ orbitally excited B states are expected. The limited statistics of the present data sample and the large number of states do not permit detailed measurements of all possible parameters. Nevertheless, it is found that the mass of the narrow doublet (here parametrized by the B_2^* mass) and the overall production rate of the four B^{**} states can be determined from the data, under reasonable assumptions provided by HQS.

The mass $M(B_2^*)$ and the total number of signal events are taken as free parameters to be determined from a fit to the $B\pi$ mass spectrum. All other parameters used for the B^{**} states are guided by theory [1, 2] and are detailed in table 1. The B_2^*, B_1 mass difference ($12\,\mathrm{MeV/c^2}$) and widths, and the equality of the B_2^* branching ratios to $B^*\pi$ and $B\pi$, are as calculated in [2]. The masses and widths of the two wide states correspond to rough theoretical expectations [1]; these are not very precise due to the absence of experimental information on the wide states in the D^{**} system. The relative production rates of the four states are set according to the spin counting factor of $2J+1$, where J is the total spin. The absence of the decays $B_1 \to B\pi$, $B_1^* \to B\pi$ and $B_0 \to B^*\pi$ follows from angular momentum and parity conservation.

The fit follows the procedure outlined in section 4.2, with the signal represented by a sum of five Breit-Wigners corresponding to the decays $B_2^* \to B\pi$, $B_2^* \to B^*\pi$, $B_1 \to B^*\pi$, $B_1^* \to B^*\pi$ and $B_0 \to B\pi$. The Breit-Wigner functions for the broad states include a mass-dependent width

State	$J^P_{j_q}$	Mass (MeV/c^2)	Full Width Γ (MeV/c^2)	relative production rate	BR($B\pi$)	BR($B^*\pi$)
B_2^*	$2^+_{3/2}$	$M(B_2^*)$	25	5/12	0.5	0.5
B_1	$1^+_{3/2}$	$M(B_2^*) - 12$	21	3/12	0.0	1.0
B_1^*	$1^+_{1/2}$	$M(B_2^*) - 100$	150	3/12	0.0	1.0
B_0	$0^+_{1/2}$	$M(B_1^*) - 12$	150	1/12	1.0	0.0

Table 1: Properties, relative production rates and branching ratios of the four B^{**} states used in the fit.

to suppress decays at their kinematic threshold. The $B\pi$ mass spectra for the $B^{**} \to B^*\pi$ decays are displaced downward by 46 MeV/c^2 due to the missing soft photon from the $B^* \to B\gamma$ decay.

The B_2^* mass $M(B_2^*)$ and the total area A_{BW} of the five Breit-Wigners are determined to be: $M(B_2^*) = (5739^{+\ 8}_{-11})\,\mathrm{MeV/c^2}$ and $A_{BW} = 45 \pm 13$ events. In Fig. 4a, the $B\pi$ mass distribution in the data is superimposed on the corresponding distribution from the fit which includes the four B^{**} states plus the expected background. It can be seen from Fig. 4a that the data are compatible with the HQS model of the $\ell = 1$ orbitally excited B^{**} system. An expanded view of the signal region, showing the contributions from each of the five decay channels, is displayed

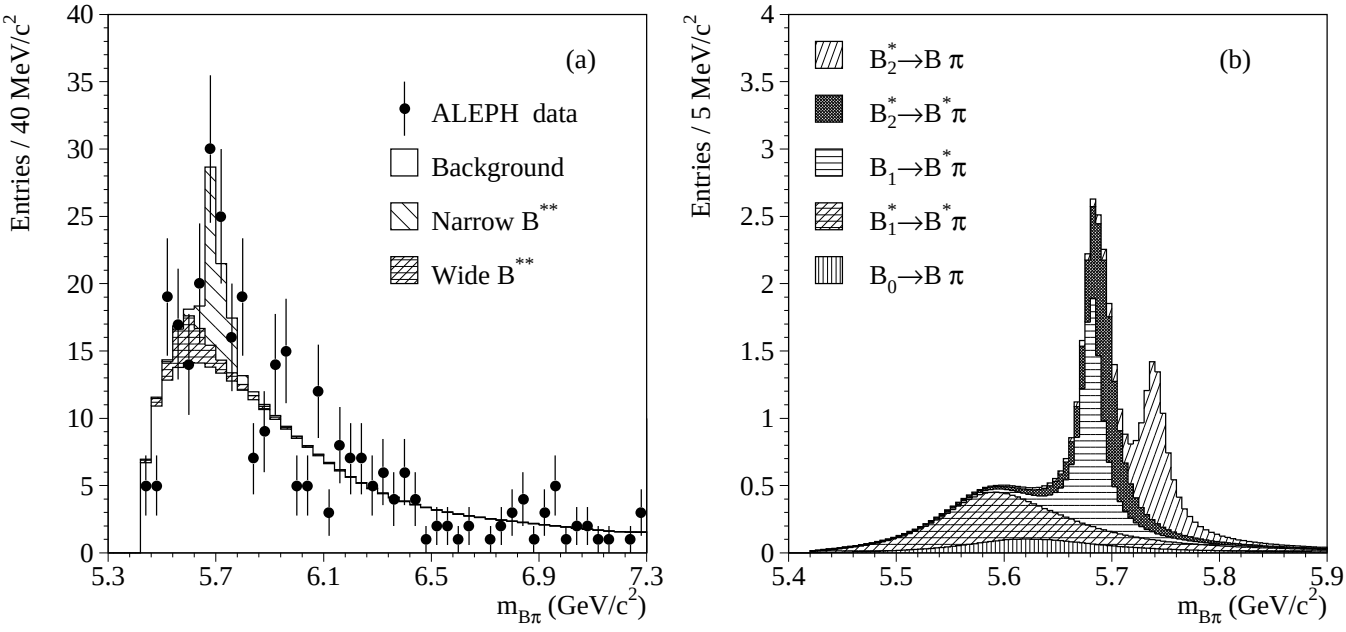

Figure 4: (a) The $B\pi$ mass spectrum from data (points with error bars) and fit (histogram). The fit includes the expected background plus contributions from the narrow and wide B^{**} states as described in the text. (b) An expanded view of the signal region, showing the contributions to the $B\pi$ mass spectrum from the five B^{**} decay channels.

in Fig. 4b.

Under the assumption that the observed signal, as measured by the total area of the five Breit-Wigner functions, is due to B^{**} production and subsequent decay to $B^{(*)}\pi$, the relative production rate is determined to be $f_{B^{**}} = (31 \pm 9)\%$. As with the Gaussian fit in section 4.2, the calculation of $f_{B^{**}}$ takes account of the efficiency of the P_L^{max} algorithm, the B purity, and an isospin factor of 2/3. A small correction for the presence of $B_s^{**} \to BK^{\pm}$ decays [3] is also included.

Systematic uncertainties on $M(B_2^*)$ and $f_{B^{**}}$ are tabulated in table 2. The assumed parameters of the B^{**} system, and the mass cut used for normalization, are varied as indicated. The effect of changing from spin to state counting (equal production rates for the four B^{**} states), and varying the efficiency of the P_L^{max} algorithm, the B purity and the B_s^{**} production rate within their errors are also listed, as well as the background shape uncertainty. The final values are:

$$M(B_2^*) = (5739^{+\ 8}_{-11}(\text{stat})^{+6}_{-4}(\text{syst}))\,\text{MeV/c}^2$$

$$f_{B^{**}} \equiv \frac{BR(b \to B^{**} \to B^{(*)}\pi)}{BR(b \to B_{u,d})} = (31 \pm 9(\text{stat})^{+6}_{-5}(\text{syst}))\%.$$

The result for the mass of the B_2^* state is somewhat low compared to the predicted value of $5771\,\text{MeV/c}^2$ given in reference [2]. Similar observations were also reported by the inclusive analyses [3, 4, 5].

Source of uncertainty	$\Delta(f_{B^{**}})$ (%)	$\Delta M(B_2^*)$ (MeV/c^2)
Γ of wide states: $100 \to 400\,\text{MeV/c}^2$	± 1	± 1
Γ of narrow states: $\pm 10\,\text{MeV/c}^2$	± 3	± 1
$M(B_2^*) - M(B_1^*)$: $50 \to 150\,\text{MeV/c}^2$	± 1	± 1
$M(B_2^*) - M(B_1)$: $6 \to 18\,\text{MeV/c}^2$	± 1	$^{+1}_{-4}$
Spin $\to$ state counting	$+3$	$+6$
BR($B_2^* \to B\pi$): 0.3$\to$0.7	± 1	± 1
Efficiency of the P_L^{max} algorithm	± 2	-
Background shape	± 2	-
Purity of the B sample	± 1	-
Normalisation mass cut: $5.9 \to 6.2\,\text{GeV/c}^2$	± 1	-
B_s^{**} production	± 1	-
Total systematic uncertainty	$^{+6}_{-5}$	$^{+6}_{-4}$

Table 2: Systematic uncertainties and their effect on the relative production rate of the B^{**} states and the mass of B_2^*.

5 B Flavour Tagging

Flavour tagging is expected to play an important role in future CP violation experiments in the b-quark sector [11]. In one class of these experiments, neutral B mesons, decaying into a CP eigenstate such as $J/\psi K^0_s$, must be tagged at production as a B^0 or $\bar{B}^0$. CP violation will lead to an asymmetry in the B^0, $\bar{B}^0$ decay rates which is a sinusoidal function of proper time.

In this section, the use of the P_L^{max} track, chosen from the tracks which pass the general selection of section 4.1, is examined as a flavour tag. The charge-flavour correlations that make this tag effective have contributions both from string fragmentation, and from the $B^{**} \to B\pi^{\pm}$ decays described in section 4. The efficiency and purity of the P_L^{max} tag are determined in the data for both neutral and charged B's, and then compared to the corresponding results from simulation. The same tag may be of use in the future CP violation experiments, but the detailed results will differ, due to the different B production dynamics and backgrounds.

The sign of the tag is measured by correlating the flavour of the B at decay (determined from its decay products) with the charge of the P_L^{max} pion: a π^+ right-sign tags a B^0, etc., according to the prescription given in section 4.1. In the case of neutral B decays, $B^0 - \bar{B}^0$ mixing induces an asymmetry between right-sign and wrong-sign tags which is a sinusoidal function of the B decay proper time.

5.1 Tagging Neutral B Mesons

In the sample of 166 neutral B candidates, 147 have a tagging track, leading to a tagging efficiency:

$$\epsilon^N_{tag} = (89 \pm 3(\text{stat}) \pm 2(\text{syst}))\,\% ,$$

where the systematic error comes from the uncertainty due to the fake B's in the sample.

The asymmetry $\mathcal{A}^N$ between the number of right-sign and wrong-sign tags, $\mathcal{A}^N = (N_{rs} - N_{ws})/(N_{rs} + N_{ws})$, is shown as a function of the B decay proper time, t, in Fig. 5a. The sinusoidal mixing of B^0 into $\bar{B}^0$ gives rise to the excess of wrong-sign tags (negative value of $\mathcal{A}^N$) at high proper times.

The physical quantities of interest are ω^N_{tag}, the mistag rate for neutral B's, which is measured from the oscillation amplitude, and Δm_d, the mass difference of the CP eigenstates, which sets the oscillation frequency. The value of ω^N_{tag} is extracted from the data of Fig. 5a with an unbinned likelihood fit. The value of Δm_d is fixed to the world average of $0.474 \pm 0.031\,\text{ps}^{-1}$ [10] during the fit.

The likelihood function is constructed by multiplying together the individual event probabilities $\mathcal{P}_i$ that event i has a measured tag μ_i at proper decay time t_i, with $\mu_i = +1$ for a right-sign tag and -1 for a wrong-sign tag. Taking account of the fake B's with their own lifetime component, this probability can be expressed as:

$$\mathcal{P}_i = [(1-\omega^N_{tag})\frac{1}{\tau_B}e^{-t_i/\tau_B}\frac{1+\mu_i\cos(\Delta m_d t_i)}{2} + \omega^N_{tag}\frac{1}{\tau_B}e^{-t_i/\tau_B}\frac{1-\mu_i\cos(\Delta m_d t_i)}{2}]f_B + \frac{1}{\tau_f}e^{-t_i/\tau_f}\frac{1+\mu_i\mathcal{A}_f}{2}f_f\,, \quad (1)$$

where $\tau_B = 1.56 \pm 0.06\,\mathrm{ps}$ [10] is the B^0 lifetime, $f_f = 1 - f_B = 0.14 \pm 0.03$ is the impurity of the sample, $\tau_f = 1.0 \pm 0.5\,\mathrm{ps}$ is the lifetime of the fake B's [9], and $A_f = -0.08 \pm 0.05$ is the asymmetry of the fake B's (estimated from the sample of fake B's in the data). The fit gives:

$$\omega^N_{tag} = (34.4 \pm 5.5(\mathrm{stat}) \pm 1.0(\mathrm{syst}))\,\%\,.$$

The systematic uncertainty was estimated by varying all other parameters within their errors. Table 3 summarises the individual contributions. The probability that a random tag ($\omega^N_{tag} = 50\%$) would give the measured value (or less) is 4×10^{-3}. This indicates that a tag based on the charge of the near-by pion can successfully tag the flavour of neutral B mesons.

In terms of the measured and fitted quantities, the asymmetry $\mathcal{A}^N$ can be written as:

$$\mathcal{A}^N(t) = \frac{\mathcal{A}_f f_f \frac{e^{-t/\tau_f}}{\tau_f} + (1-2\omega^N_{tag})f_B\frac{e^{-t/\tau_B}}{\tau_B}\cos(\Delta m_d t)}{f_f\frac{e^{-t/\tau_f}}{\tau_f} + f_B\frac{e^{-t/\tau_B}}{\tau_B}}\,. \quad (2)$$

The corresponding curve from the fit is overlaid on the data in Fig. 5a.

Source of uncertainty	$\Delta\omega^N_{tag}$ (%)	$\Delta\omega^C_{tag}$ (%)
Purity of the B sample (f_B)	0.7	0.3
Asymmetry from fake B's (A_f)	0.5	0.5
lifetime of fake B's (τ_f)	0.2	0.2
lifetime of B's (τ_B)	0.0	0.0
mass difference (Δm_d)	0.5	-
Total systematic uncertainty	1.0	0.7

Table 3: Systematic uncertainties on the mistag rates ω^N_{tag} and ω^C_{tag}.

5.2 Tagging Charged B Mesons

As a further check on the charge-flavour correlations associated with the P_L^{max} pion tag, the tagging of $B^\pm$ decays is studied. In the case of the 238 fully reconstructed charged B mesons, 212 have a tagging track. Thus the tagging efficiency is

$$\epsilon^C_{tag} = (89 \pm 2(\mathrm{stat}) \pm 1(\mathrm{syst}))\,\%.$$

Equations (1) and (2) also hold for charged B's with the obvious change that $\Delta m_d = 0$ (and N is replaced by C). The asymmetry $\mathcal{A}^C(t)$ is plotted in Fig. 5b. Only a weak dependence on

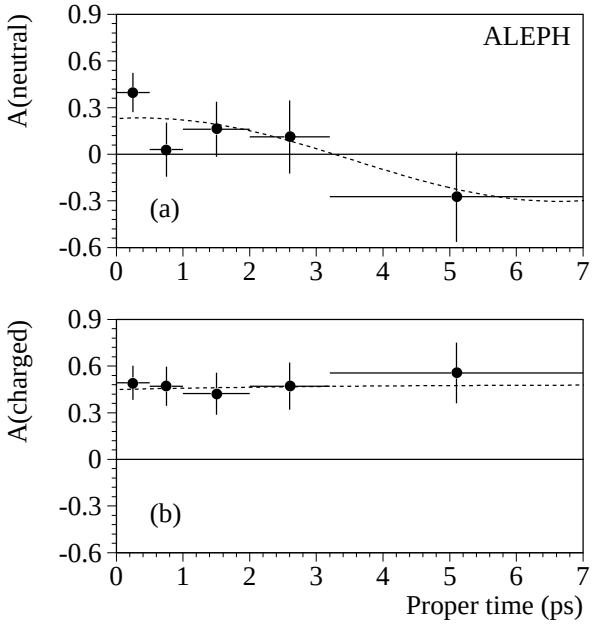

Figure 5: The right-sign/wrong-sign asymmetries in the data as a function of the proper decay time. The dashed curves display the charge asymmetries (equation 2) determined from the unbinned likelihood fits. (a) Neutral B mesons; the dashed curve shows $\mathcal{A}^N$ with $\omega^N_{tag} = 34.4\%$ and Δm_d equal to the world average. (b) Charged B mesons; the dashed curve shows $\mathcal{A}^C$ with $\omega^C_{tag} = 26.0\%$ and $\Delta m_d = 0$.

the B decay proper time is expected in this case, due to the different lifetime of the fake B's. The height of the curve above zero is a measure of (1-2ω^C_{tag}). With $\tau_B = 1.62 \pm 0.06$ ps [10], $f_f = 1 - f_B = 0.16 \pm 0.03$ and $A_f = 0.35 \pm 0.05$, an unbinned likelihood fit for ω^C_{tag} gives

$$\omega^C_{tag} = (26.0 \pm 3.6(\text{stat}) \pm 0.7(\text{syst}))\,\%.$$

The corresponding fit to the data is displayed in Fig. 5b and the contributions to the systematic error are shown in table 3.

5.3 Discussion of the tagging results

The above studies were also performed in a high statistics sample of simulated events, generated with JETSET 7.4 [12], which included the production of B^{**} and B^{**}_s at the 34 % level, relative to $B_{u,d}$. The results, $\epsilon^N_{tag} = 89\,\%$, $\omega^N_{tag} = 36\,\%$ for the neutral B's and $\epsilon^C_{tag} = 90\,\%$, $\omega^C_{tag} = 32\,\%$ for charged B's, are in agreement with the values measured in the data, suggesting that the model of string fragmentation plus B^{**} production and decay reproduce reasonably well the existing charge-flavour correlations. Switching off the B^{**} production in the simulation degrades slightly the above results, but significant correlations still remain due to the fragmentation process. This was also observed in the data by restricting the tagging pions to tracks with $B\pi^{\pm}$ invariant mass above 6 GeV/c^2.

Finally, the difference in the mistag rates between charged and neutral B's clearly seen in the simulation (the data show the same trend but the uncertainties are too large to allow any definite conclusions to be drawn) was traced to strange quark production in fragmentation, which spoils the isospin symmetry between the u and d quarks in favour of the charged B's [13]. In the simulation, rejecting tags from charged tracks misidentified as pions (mostly $K^{\pm}$), leads the mistag rates for charged and neutral B's to converge. Therefore, in the absence of perfect pion-kaon separation, the charged B's cannot be used to infer results for the neutral B's.

6 Conclusions

A sample consisting of 404 fully reconstructed B mesons originating from hadronic Z decays was used to search for resonant production in the $B\pi^{\pm}$ system. Combining the B meson with the right-sign P_L^{max} charged pion, a structure is observed above the expected background in the $B\pi$ mass spectrum. A mass of $(5695^{+17}_{-19})\,\mathrm{MeV/c^2}$, a width of $(53^{+26}_{-19})\,\mathrm{MeV/c^2}$ and a relative production rate of $(30^{+12}_{-10}(\mathrm{stat}) \pm 3(\mathrm{syst}))\%$ are determined from a single Gaussian fit. These results are consistent with previous observations [3, 4, 5] and with Heavy Quark Symmetry (HQS) expectations for the production of B^{**} states decaying into $B^{(*)}\pi^{\pm}$ [2]. In the framework of HQS, the total production rate of the B^{**} states is determined to be $BR(b \to B^{**} \to B^{(*)}\pi)/BR(b \to B_{u,d}) = (31 \pm 9(\mathrm{stat})^{+6}_{-5}(\mathrm{syst}))\%$ and the mass of the B_2^* state $M(B_2^*) = (5739^{+\ 8}_{-11}(\mathrm{stat})^{+6}_{-4}(\mathrm{syst}))\,\mathrm{MeV/c^2}$.

Using the same sample of reconstructed B's, the efficiency and purity of a flavour-tag with a near-by pion are determined. This technique may well play an important role in future studies of $B - \bar{B}$ mixing and CP violation in the B system, as first suggested in [1]. The specific tag that is used is based on the charge of the pion with the highest longitudinal momentum, relative to the B direction. It is found that it is possible to flavour-tag both charged and neutral B's in this way with high efficiency and a reasonable mistag rate. This P_L^{max} tag, which is based on tracks in the same jet as the B, can be used as a tag which is independent of tags based on track(s), such as a high p_t lepton, in the opposite jet. It can thus be used to increase the overall tagging ability and cross-check the performance of the other tags.

Acknowledgements

We wish to thank our colleagues in the CERN accelerator divisions for the successful operation of LEP. We are indebted to the engineers and technicians in all our institutions for their contributions to the excellent performance of ALEPH. Those of us from non-member states warmly thank CERN for its hospitality.

References

[1] M. Gronau, A. Nippe and J. Rosner, Phys. Rev. D **47** (1993) 1988;
M. Gronau and J. Rosner, Phys. Rev. D **49** (1994) 254;
M. Gronau and J. Rosner, Phys. Rev. Lett. **72** (1994) 195.

[2] E.J. Eichten, C.T. Hill and C. Quigg, Phys. Rev. Lett. **71** (1993) 4116 and an update FERMILAB-CONF-94/118-T.

[3] OPAL Collaboration, *Observations of $\pi - B$ charge-flavor correlations and resonant $B\pi$ and BK production*, Z. Phys. C **66** (1995) 19.

[4] DELPHI Collaboration, *Observation of orbitally excited B mesons*, Phys. Lett. B **345** (1995) 598.

[5] ALEPH Collaboration, *Production of Excited Beauty States in Z Decays*, Z. Phys. C **69** (1996) 393.

[6] ALEPH Collaboration, *ALEPH: A detector for electron-positron annihilations at LEP*, Nucl. Instr. Meth. A **294** (1990) 121.

[7] ALEPH Collaboration, *Performance of the ALEPH detector at LEP*, Nucl. Instr. Meth. A **360** (1995) 481.

[8] B. Mours et al. , Nucl. Instr. Meth. A **379** (1996) 101.

[9] ALEPH Collaboration, *Improved Measurement of the $\bar{B}^0$ and B^- Meson Lifetimes*, Z. Phys. C **71** (1996) 31.

[10] Particle Data Group, Phys. Rev. D **54** (1996) 1.

[11] J. Boudreau, proceedings of the 28th International Conference on High Energy Physics, Warsaw, Poland, 25–31 July, 1996. Eds. Z. Ajduk and A.K. Wróblewski, World Scientific (1997), p. 1224;
P. Eerola, Nucl. Instr. Meth. A **384** (1996) 93;
A. Kharchilava, Nucl. Instr. Meth. A **384** (1996) 100;
I. Abt, Nucl. Instr. Meth. A **384** (1996) 113.

[12] T. Sjostrand and M. Bengtsson, Comput. Phys. Commun. **43** (1987) 367.

[13] I. Dunietz and J. L. Rosner, Phys. Rev. D **51** (1995) 2471.